J Mater Sci: Mater Electron (2022) 33:15665–15678

Design and synthesis of novel bichalcophene derivatives with double anchoring groups for dye-sensitized solar cell applications: sensitization and co-sensitization with N-719

Fatma H. Abdelhamed[1], Mohamed A. Ismail[1], Ehab Abdel-Latif[1], Ayman A. Abdel-Shafi[2], and Mohamed R. Elmorsy[1,*]

[1] Department of Chemistry, Faculty of Science, Mansoura University, El-Gomhoria Street, Mansoura 35516, Egypt
[2] Department of Chemistry, Faculty of Science, Ain Shams University, Abbassia, Cairo 11566, Egypt

Received: 6 February 2022
Accepted: 24 May 2022
Published online: 8 June 2022

ABSTRACT

Novel dyes **F1-3** based on bichalcophene-pyrimidine-2,4,6-trione derivatives with dual anchoring were developed, synthesized, and evaluated as sensitizers and co-sensitizers for dye-sensitized solar cells (DSSCs). **F1** displayed the best DSSC performance (η, PCE = 4.41%) and the highest photovoltaic parameters, which were as follows: current density, J_{SC} = 10.66 mA cm^{-2}, photovoltage, V_{OC} = 0.654 V, and fill factor, FF = 64.3%. These findings can be ascribed to **F1**'s superior optical and electrochemical characteristics when compared to other structures such as **F2** and **F3**. Interestingly, devices that rely on the **F1 + N-719** co-sensitization approach had greater photocurrent and photovoltage than the standard **N-719** dye, generating a power conversion efficiency (PCE) of 9.97%. This improved performance was mostly due to a higher J_{SC} value of 23.28 mA cm^{-2} for the dye **F1** and a maximum molar extinction coefficient in the 350–550 nm region, which enhanced the light-harvesting capacity of the **N-719** dye.

1 Introduction

Once the published work in 1991 by O'regan and Grätzel, who used a trimeric ruthenium structure adsorbed on the nanoporous edge of a semiconductor (Titanium dioxide) to achieve PCE over 7.12%, dye-sensitized solar cells (DSSCs) gave rise to a new, low-cost, and high-power conversion efficiency (PCE) devices around 1991, making a case for the origins of photovoltaic (PV) cells [1]. As a result of this research, scientists have concentrated considerable effort on developing new structures with higher PCE. Small organic compounds [2, 3], porphyrins [4, 5], and ruthenium compounds [6, 7] have all been employed as DSSCs. The metal-to-ligand charge-transfer

Address correspondence to E-mail: m.r.elmorsy@gmail.com

https://doi.org/10.1007/s10854-022-08470-9

(MLCT) transition is responsible for the absorption of common ruthenium-based dyes (N-719, N-749, N3, and so on) over a broad wavelength range of 350 to 900 nm [6–8]. Metals' usage in DSSCs on a broad scale is limited due to their elevated manufacturing resources and environmental impacts [9]. To achieve an effective electrical transfer between dye and semiconductor, novel metal-free dyes with maximum molar absorptivity coefficients, a broad range of light absorption, and high reliability to absorb on the surface of TiO_2 are needed [10]. On the other hand, metal-free organic dyes have various benefits over the previous class, including simple availability, design diversity, high molar extinction coefficients, adjustable absorption spectrum range from visible to near-infrared (NIR), and low cost of fabrication [11–13]. Consequently, large numbers of metal-free organic dyes have been created and explored as prospective DSSC photosensitizers, and system efficiency connections have been discovered [14, 15]. When utilized in DSSCs, several metal-free dyes based on indole, phenoxazine, carbazole, thiophene, and phenothiazine, are good sensitizers with good photovoltaic performance. A thiophene core has been recognized as a viable entity among the above-mentioned heterocyclic compounds because of its adjustable electrochemical and spectroscopic properties [16–19].

Also, the chemical structure of dyes should have specific functional group, which act as anchoring moieties for binding the dye to the semiconductor surface. Several published photosensitizers possessing cyanoacetic acid, barbituric acid, and rhodamine cores were exposed to be efficient anchoring units [20, 21]. Nonetheless, the majority of those organic compounds have a single anchor, and there have been few investigations into dual-tethered organic dyes for co-sensitizing ruthenium dyes. Dual-anchored dyes have a tighter link to the photoanode and an electrostatic repulsion with efficient prevention of intermolecular accumulation that reduces electron recombination processes as compared to single-anchored dyes [22, 23]. As shown in Fig. 1, novel organic compounds with dual anchoring functionalities are presented. The framework was used to construct three novel bichalcophene-pyrimidine-2,4,6-trione-based sensitizers, **F1**, **F2**, and **F3**, incorporating dual anchoring moieties of barbituric analogs. A comparative study of the photophysical, electrochemical, and photovoltaic characteristics of three bichalcophene derivatives was carried out. Figure 1 illustrates the molecular architecture of **F1**, **F2**, and **F3**. Co-sensitization is a very good approach for improving the light-harvesting potential of DSSCs using two or more organic dyes within the same fabricating device [24, 25]. Several essential characteristics must be met to fabricate a co-sensitization system with high performance: (1) The co-sensitizers should have structural properties that reduce dye incorporation within the semiconductor film; (2) they should have high molar extinction coefficients (ε) that can compensate for the main sensitizer's lack of an absorption spectrum; and (3) a small structure of co-sensitizers is preferred to fill the void left by the main sensitizer [26–28]. Furthermore, in order to be commercialized, organic dyes must have a basic structure, be straightforward to synthesis with a few processes, and offer distinct features like configurable molecular architecture, cheap cost, adaptable electrochemical, and absorption characteristics. The simple structure of bichalcophene sensitizers (**F1-3**), consists of segments that, are widely used in the manufacture of most efficient DSSCs dye-sensitized solar cells and charge transport materials [29], π-conjugation represented in bithiophene and bifuran moieties, and the dual anchoring dyes (1,3-dimethyl are preferred to monoanchoring dyes mainly due to certain favorable inherent properties. As a result, we combined the new dyes with **N-719** (Fig. 1), a conventional great-efficiency bipyridyl Ru (II) photosensitizer, to improve the photovoltaic performance of DSSCs with complementing optical absorption [30] and explore their photovoltaic capabilities further. Interestingly, in the co-sensitization process, all photovoltaic parameters, including photovoltage, photocurrent, and fill factor, are enhanced.

2 Synthesis

2.1 Preparation of 5-arylidine-1,3-dialkylbarbituric acids 3a,b

2.1.1 5-[(5-Bromothiophen-2-yl)methylene]-1,3-dimethylpyrimidine-2,4,6-trione (3a)

To a solution of 1,3-dimethylbarbituric acid (4.68 g, 30 mmol) and 5-bromothiophene-2-carboxaldehyde (5.73 g, 30 mmol) in methanol (50 mL) was added few drops of conc. HCl. The reaction mixture was

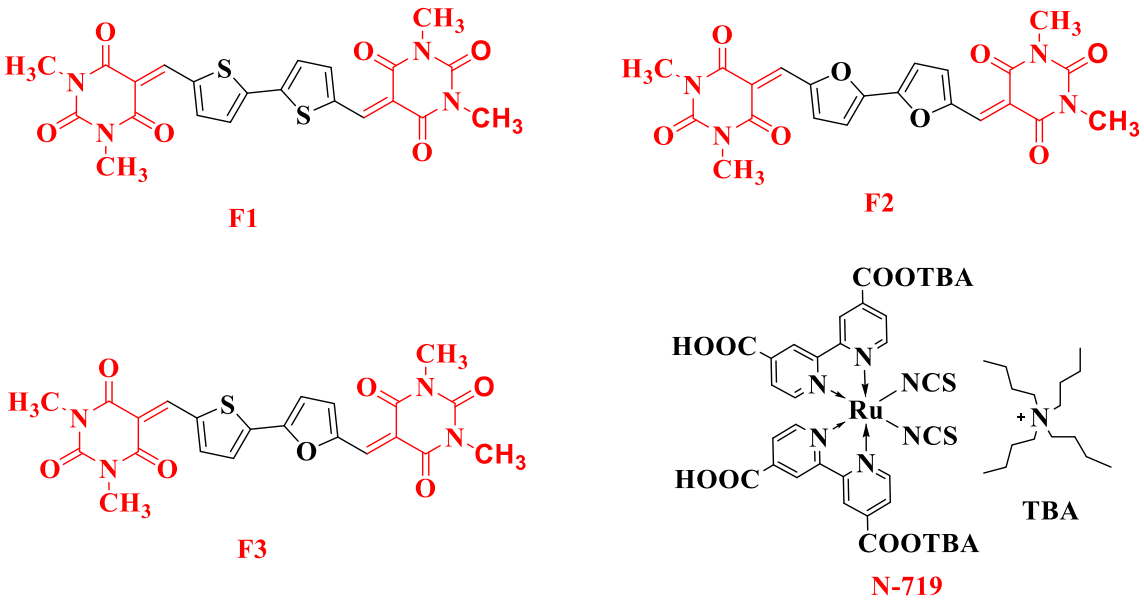

Fig. 1 Molecular structures of compounds **F1-3** and **N-719** [31]

heated at reflux for 3 h and the precipitate was filtered off, washed with methanol and recrystallized from ethanol/EtOAc to afford compound **3a**. Yield 81%, mp 248–250 °C. IR (KBr) ν' 3095, 3072 (sp^2 C–H), 2990, 2949 (sp^3 C–H), 1727, 1660 (CO), 1540, 1493 (C=C) cm^{-1}. ^{1}H-NMR (DMSO-d_6); δ 3.21 (s, 6H; 2 × N-CH_3), 7.53 (d, J = 4.2 Hz, 1H, thiophene H's), 8.04 (d, J = 4.2 Hz, 1H, thiophene H's), 8.52 (s, 1H, methine H's). MS (EI) m/e (rel.int.); 328, 330 (M^+, 8; Br isotopes), 249 (30), 56 (100). Anal. Calc. for $C_{11}H_9BrN_2O_3S$ (329.17): C, 40.14; H, 2.76; N, 8.51. Found: C, 39.89; H, 2.85; N, 8.60.

2.1.2 5-[(5-Bromofuran-2-yl)methylene]-1,3-dimethylpyrimidine-2,4,6-trione (3b)

Compound **3b** was obtained adopting the same methodology used for preparation of **3a**, starting with 5-bromofuran-2-carboxaldehyde instead of 5-bromothiophene-2-carboxaldehyde. Yield 86%, mp 196–198 °C. IR (KBr) ν' 3178, 3132 (sp^2 C–H), 2995, 2952 (sp^3 C–H), 1725, 1662 (CO), 1572, 1412 (C=C) cm^{-1}. ^{1}H NMR ($CDCl_3$); δ 3.39, 3.41 (2 s, 6H; 2 × N-CH_3), 6.69 (d, J = 3.9 Hz, 1H, furan H's), 8.34 (s, 1H, methine H's), 8.60 (d, J = 3.9 Hz, 1H, furan H's). MS (EI) m/e (rel.int.); 312, 314 (M^+, 6; Br isotopes), 233 (100), 176 (53). Anal. Calc. for $C_{11}H_9BrN_2O_4$ (313.10): C, 42.20; H, 2.90; N, 8.95. Found: C, 42.03; H, 3.05; N, 8.89.

2.2 General procedure for preparation of bichalcophene-5,5′-bis-(methylidenes) bis-1,3-dialkylbarbituric acids F1 and F2

2.2.1 5,5′-[2,2′-Bithiophene-5,5′-diylbis(methylidene)]-bis-(1,3-dimethylpyrimidine-2,4,6-trione) (4a, F1)

To a solution of bromo compound **3a** (1.56 g, 5 mmol), and $Pd(PPh_3)_4$ (200 mg) in toluene (40 mL) was added hexa-*n*-butylditin (2.9 g, 5 mmol). The reaction mixture was heated under N_2 at 120 °C for 12 h, then the precipitate was filtered and washed with hexanes, recrystallized from DMF to give compound **4a** in 79% yield, mp > 300 °C, lit. mp. 438 °C [32]. IR (KBr) ν' 3080 (sp^2 C–H), 2957 (sp^3 C–H), 1723, 1657 (CO), 1551, 1461 (C=C) cm^{-1}. ^{1}H-NMR (TFA-*d*, CF_3COOD); δ 3.50, 3.52 (2 s overlapped, 12H, 4 × N-CH_3), 7.76 (d, J = 4.0 Hz, 2H, thiophene H's), 8.01 (d, J = 4.0 Hz, 2H, thiophene H's), 8.90 (s, 2H, methine H's), MS (EI) m/e (rel.int.); 498 (M^+, 100), 466 (5), 328 (9), 249 (16). Anal. Calc. for $C_{22}H_{18}N_4O_6S_2$ (498.53): C, 53.00; H, 3.64; N, 11.24. Found: C, 52.74; H, 3.71; N, 11.12.

2.2.2 5,5′-[2,2′-Bifuran-5,5′-diylbis(methylidene)]-bis-(1,3-dimethylpyrimidine-2,4,6-trione) (4b, F2)

Compound **4b** was obtained adopting the same procedure used for the preparation of compound **4a**

using bromo compound **3b** instead of **3a**. Yield 73%, mp > 300 °C (DMF). IR (KBr) ν' 3174, 3113 (sp^2 C–H), 2956 (sp^3 C–H), 1728, 1663 (CO), 1571, 1463 (C=C) cm^{-1}. ^{1}H-NMR (TFA-*d*, CF_3COOD); δ 3.51 (s, 12H, 4 × N-CH_3), 7.38 (d, J = 4.0 Hz, 2H, furan H's), 8.60 (s, 2H, methine H's), 8.73 (d, J = 4.0 Hz, 2H, furan H's). MS (EI) m/e (rel.int.); 466 (M^+, 12), 270 (100). HRMS calc. for $C_{22}H_{19}N_4O_8$ (MH^+): 467.1190. Observed: 467.1203. Anal. Calc. for $C_{22}H_{18}N_4O_8$ (466.41): C, 56.65; H, 3.89; N, 12.01.Found: C, 56.46; H, 4.03; N, 12.07.

2.2.3 *5-((5-(5-((1,3-dimethyl-2,4,6-trioxotetrahydropyrimidin-5(2H)-ylidene)methyl)furan-2 yl)thiophen-2-yl)methylene)-1,3-dimethylpyrimidine-2,4,6(1H,3H,5H)-trione (7, F3)*

Firstly; 5-(5-formyl-2-thienyl)-2-furaldehyde **6** was prepared adopting a Suzuki cross coupling conditions [33], reacting 5-bromothiophenealdehyde (5 mmol) with 5-formyl-furanboronic acid (6 mmol) in 1,4-dioxane and $Pd(PPh_3)_4$ as a catalyst and anhydrous K_2CO_3 as a base. The dialdehyde **6** was attained 78% yield as a yellow solid, mp 184–185 °C and it was identical with the reported literature [34]. Secondly, dialdehyde compound **6** (1 mmol) was condensed with 1,3-dimethylbarbituric acid (2 mmol) in 30 mL methanol/acetic acid (2:1) under reflux for 24 h. The resultant precipitate was filtered off while hot. The precipitate was recrystallized from DMF to furnish compound **7** in 69% yield, mp > 300 °C. IR (KBr) ν' 2925 (sp^3 C–H), 1725, 1660 (CO), 1557, 1463 (C=C) cm^{-1}. ^{1}H-NMR (TFA-*d*, CF_3COOD); δ 3.50, 3.52 (two s overlapped, 12H; 4 × N-CH_3), 7.32–7.37 (m, 1H), 7.77–7.80 (m, 1H), 7.99–8.02 (m, 1H), 8.61 (s, 1H), 8.74 (s, 1H), 8.92–8.94 (m, 1H). MS (EI) m/e (rel.int.); 482 (M^+, 55), 466 (18), 449 (16), 66 (100). Anal. Calc. for $C_{22}H_{18}N_4O_7S$ (482.46): C, 54.77; H, 3.76; N, 11.61.Found: C, 54.91; H, 3.87; N, 11.40.

3 Results and discussion

3.1 Chemistry

Preparation of the new bithiophene-pyrimidine-2,4,6-trione derivative **4a (F1)** began with Knoevenagel condensation reaction by treatment of 5-bromothiophene-2-carboxaldehyde with 1,3-dimethylbarbituric acid to afford the bromo compound **3a,** followed by a stille-type homocoupling reaction using hexabutylditin mediated homocoupling conditions [35] for **3a** in the presence of catalytic $Pd(PPh_3)_4$ using refluxing toluene as a solvent to afford the desired compound **F1**. Adopting the same methodology used for the preparation of **3a**, starting with 5-bromofuran-2-carboxaldehyde instead of 5-bromothiophene-2-carboxaldehyde to afford the bromo compound **3b**, which also underwent a stille homocoupling reaction to afford the anticipated bifuran-pyrimidine-2,4,6-trione derivative **4b** (**F2**) as outlined in Scheme 1. The newly synthesized bichalcophene-pyrimidine-2,4,6-trione derivatives were established via their corresponding spectral analysis. In all cases, the IR spectra of the derivative products reported the existence of carbonyl groups. ^{1}H-NMR spectrum of bromothiophene methylene-1,3-dimethylbarbituric acid **3a** displayed a singlet signal characteristic of the 1,3-dimethylbarbituric acid moiety at δ 3.21 (6H), two doublet signals of the thiophene moiety at δ 7.53 and 8.04 (each signal integrated for one proton), in addition to a singlet signal of methine proton at δ 8.52 (1H), and its mass spectrum exhibited a molecular ion peak at m/z 328, 330 of bromine isotopes and a fragment peak at m/z 249 formed from the parent molecular ion through losing bromine. Moreover, the ^{1}H-NMR spectrum of the bithiophene-pyrimidine-2,4,6-trione derivative **F1** showed two singlet overlapped signals integrated for 12 protons characteristic for two 1,3-dimethylbarbituric acid moieties at δ 3.50 (6H) and 3.52 (6H) and a singlet signal at δ 8.90 (2H) of the methine H's; in addition to two doublet signals of the symmetrical bithiophene moiety at δ 7.76 and 8.01 (each signal integrated for two protons); and its mass spectrum showed a molecular ion peak at m/z 498 as a base peak. Further, the ^{1}H-NMR spectrum of bromofuran methylene-1,3-dimethylbarbituric acid **3b** displayed two singlet signals characteristic for the 1,3-dimethylbarbituric acid moiety at δ 3.39 (3H) and 3.41 (3H), two doublet signals of the furan moiety at δ 6.69 and 8.60 (each signal integrated for one proton), in addition to a singlet signal of methine proton at δ 8.34 (1H); and its mass spectrum showed a molecular ion peak at m/z 312, 314 of bromine isotopes and a fragment peak at m/z 233 as a base peak produced from the parent molecular ion through losing bromine. Moreover, the ^{1}H-NMR spectrum of the bifuran-pyrimidine-2,4,6-trione derivative **F2** showed singlet signal characteristics for two 1,3-

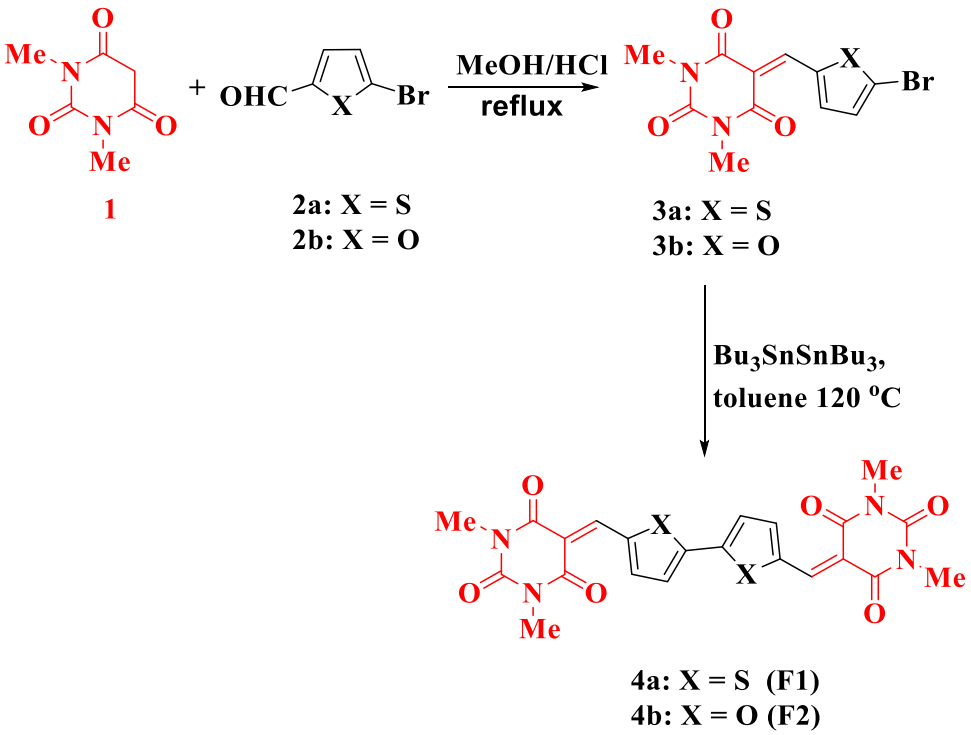

Scheme 1 Synthesis scheme for the preparation of symmetrical bichalcophene dyes **F1** and **F2**

dimethylbarbituric acid moieties at δ 3.51 (12H) and a singlet signal at δ 8.60 (2H) of the methine protons and two doublet signals of the symmetrical bifuran moiety at δ 7.38 and 8.73 (each signal integrated for two protons); and its mass spectrum showed a molecular ion peak at m/z 466 and a fragment peak at m/z 270 as a base peak.

Scheme 2 outlines the preparation of the new unsymmetrical bichalcophene dye **7** (**F3**) starting with Suzuki coupling by treatment of bromothiophene aldehyde **2a** with (5-formylfuran-2-yl)boronic acid (**5**) to furnish dialdehyde compound **6,** which is subsequently condensed with 2 equivalents of 1,3-dimethylbarbituric acid to afford the target compound **F3**. The newly synthesized bichalcophene-pyrimidine-2,4,6-trione derivative **F3** was assured based on the spectral data. Thus, the IR spectra of bichalcophene-pyrimidine-2,4,6-trione derivative **F3** indicated the presence of carbonyl groups. ^{1}H-NMR spectrum of compound **7** displayed two singlet overlapped signals characteristic of two 1,3-dimethylpyrimidine-2,4,6-trione moieties at δ 3.50 (6H) and 3.52 (6H), and four protons of thiophene and furan moieties, in addition to two singlet signals of bis methylidenes at δ 8.61 (1H) and 8.74 (1H). Additionally, its mass spectrum showed a molecular ion peak at m/z 482 (M^{+}).

3.2 Optical measurements

The UV/visible absorption spectra of dyes **F1-3** measured in DMF solution (2×10^{-5} M) are presented in Fig. 2, and their related parameters are summarized in Table 1.

Compounds **F1-3** exhibited wide absorption in the 350–550 nm region, which corresponds to the conjugated system's π–π^{*} transition and intramolecular charge transfer (ICT). Compound **F1** showed a bathochromic shift with maximum molar extinction coefficient (ε), which is explained by the availability of bithiophene in its architecture, which causes an increase in conjugation, and hence the absorption occurred at a longer wavelength [36]. $E_{0\text{-}0}$ (energy gap) was calculated from the beginning of the lowest possible-energy peak [37], and the values are **F1** (2.32 eV), **F2** (2.57 eV), and **F3** (2.33 eV), respectively, compared to the $E_{0\text{-}0}$ of **N-719** (1.92 eV). In the same spectral region, the molar extinction values obtained for **F1-3** are higher than those for **N-719** dye. Because of its complementary light-harvesting capacity, **F1-3** dye may be a good co-sensitizing option with **N-719** in DSSC. **F1-3** have maximum absorption wavelengths of 509 nm ($\varepsilon = 5.72 \times 10^{4}$ M^{-1} cm^{-1}), 512 nm ($\varepsilon = 2.11 \times 10^{4}$ M^{-1} cm^{-1}), and 514 nm ($\varepsilon = 4.17 \times 10^{4}$ M^{-1} cm^{-1}), respectively. **N-719**, on

Scheme 2 Synthesis scheme for the preparation of unsymmetrical bichalcophene dye **F3**

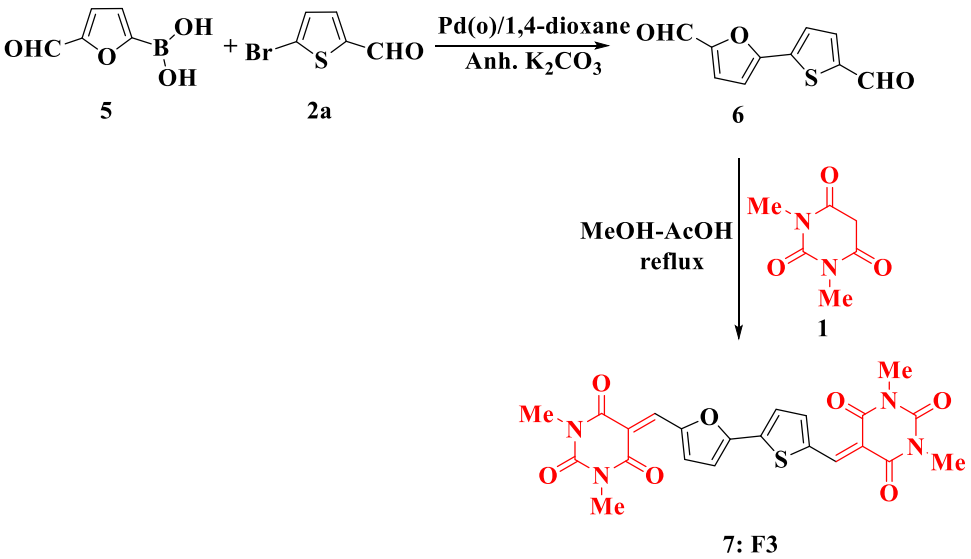

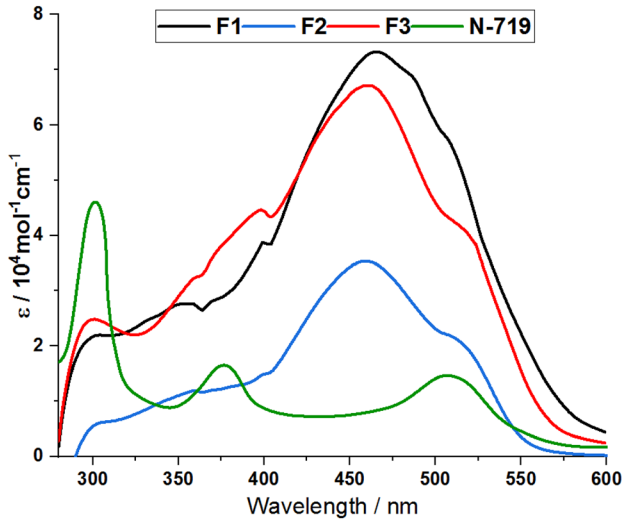

Fig. 2 Absorption spectra of bichalcophene derivatives **F1-3** in DMF

the other hand, had a maximum absorption wavelength of 512 nm ($\varepsilon = 1.42 \times 10^4\ M^{-1}\ cm^{-1}$).

Figure 3 illustrates the normalized UV/visible absorption peaks of compounds **F1-3** on TiO_2 thin film. The absorbance spectra of the solid film were wider, suggesting that the adsorption of the substance on the TiO_2 surface was in high quantities. The interaction between the Ti^{4+} ions of the semiconductor and the carbonyl group in the pyrimidine ring of the investigated compounds causes the spectra to broaden, resulting in a drop in the dye particle's π^* energy level, which is advantageous for enhancing the photovoltaic performance of the DSSCs, particularly the photocurrent [38]. The adsorption of substances on the surface of the TiO_2 appeared in the sequence **F1** > **F3** > **F2**.

Cyclic voltammetry (CV) studies are used to measure the redox potentials of structures **F1-3** in addition to the thermodynamic possibility of charge transfer [39]. To adjust the reduction potential, ferrocene (0.4 V vs. normal hydrogen electrode (NHE)) is used as an external reference. The oxidation onset of **F1-3**, which is comparable to the ground state oxidation potential (GSOP), was evaluated using CV graphs (Fig. 4). The excited state oxidation potential was calculated from the obtained GSOP and $E_{0\text{-}0}$ as shown in Eq. 1 (a value of 4.7 was added to obtain values in eV)

$$\mathrm{ESOP} = [((\mathrm{GSOP}\ (\mathrm{V}) + 4.7) - -E_{0-0}]\mathrm{eV} \quad (1)$$

Table 1 Photophysical parameters of bichalcophene derivatives **F1-3**

Structure	λ_{max} (nm)	$\varepsilon/10^4\ M^{-1}\ cm^{-1}$	λ_{onset} (nm)	Experimental $E_{0\text{-}0}$ (eV)
F1	300, 465, 509	2.17, 7.3, 5.72	534	2.32
F2	303, 458, 512	0.54, 3.52, 2.11	482	2.57
F3	300, 460, 514	2.46, 6.60, 4.17	532	2.33

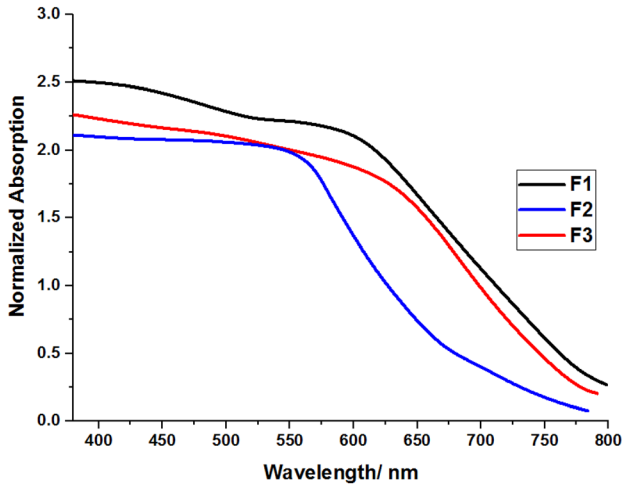

Fig. 3 Normalized Absorption of sensitized electrodes

Table 2 displays the electrochemical data obtained for structures **F1-3**. As per studies, the mechanism of successful electron injection and dye regeneration, is dependent on the relative positions of the GSOP, ESOP, conduction band (CB) of the TiO_2, and the redox potential of the electrolyte [40]. Table 2 shows that the calculated GSOP levels of dyes **F1** (− 5.82 eV), **F2** (− 6.29 eV), and **F3** (− 5.99 eV) are more positive than I_3^-/I^- redox couples (− 5.2 eV), reflecting a sufficient thermodynamic driving force for the iodine cells.

Furthermore, the ESOP levels of **F1-3** are much more negative than the CB of the TiO_2 as shown by − 3.50 eV, − 3.72 eV, and − 3.66 eV, respectively, indicating that electrons are efficiently injected from the excited dye to the CB of the TiO_2 [41]. All the dyes in the fabricated devices satisfied the basic

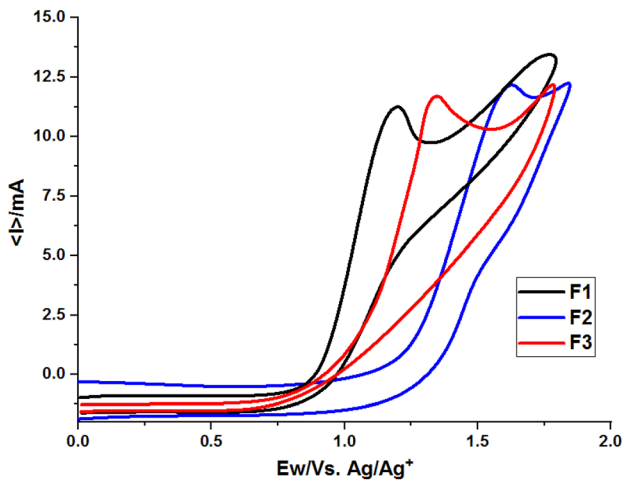

Fig. 4 Cyclic voltammograms of bichalcophene derivatives **F1-3**

Table 2 Electrochemical parameters for bichalcophene derivatives **F1-3**

Compounds	Experimental (eV)			Theoretical (eV)		
	$E_{0\text{-}0}$	GSOP	ESOP	$E_{0\text{-}0}$	GSOP	ESOP
F1	2.32	− 5.82	− 3.50	2.28	− 5.51	− 3.23
F2	2.57	− 6.29	− 3.72	2.69	− 6.34	− 3.65
F3	2.33	− 5.99	− 3.66	2.42	− 6.13	− 3.71

requirements for dye regeneration with effective electron transfer to the conduction band of the semiconductor (TiO_2) [42].

The energy level diagram of bichalcophene derivatives **F1-3** is shown in Fig. 5. The distance between both the LUMO value of dyes **F1-3** and the CB band of TiO_2 was then used to calculate the negative free energies for electron injection. Their negative free energy levels were determined to be in the following order: **F1** (0.7 eV) > **F3** (0.54 eV) > **F2** (0.48 eV). Based on the data, the highest value of **F1** indicates that its electrons are transferred with high efficiency to the CB of TiO_2.

3.3 Theoretical studies

With the Gaussian 09 at the B3LYP/6-31G* stage, the optimal geometry and electron densities of the HOMOs and LUMOs of compounds **F1-3** were examined [43]. (Figs. 6, 7).

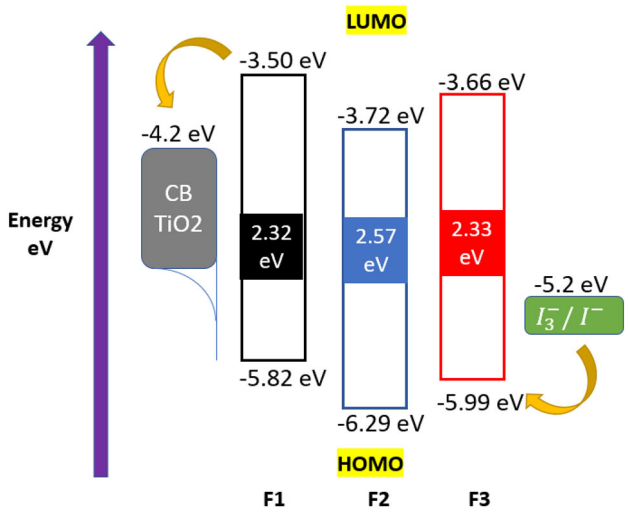

Fig. 5 Calculated energy levels for bichalcophene derivatives **F1-3**

Figure 7 shows the different behavior of the electronic distributions for the HOMO and LUMO for dyes **F1-3**. According to the results of a density functional theory investigation, the HOMO charge density of symmetrical bithiophene dye **F1** is predominantly dispersed across the bithiophene moiety, whereas the LUMO of **F1** fills up on the barbituric ring. The HOMO is present on the bifuran ring in symmetrical bifuran dye **F2**, but the LUMO is not fully extended to the barbituric ring. However, in the case of unsymmetrical bichalcophene dye **F3**, the HOMO dispersed over the thiophene-furan moiety, whereas the LUMO was found to be centered just on the barbituric ring, which was joined to the thiophene ring. In comparison to the other dyes **F2** and **F3**, these results show that **F1** has well-overlapped HOMO and LUMO molecular orbitals all over the molecules, including the two barbituric rings. Furthermore, light-illumination generated electrons in **F1** may move from dye to TiO_2 semiconductor through the HOMO–LUMO transition with high activation [44].

In this work, the molecular electrostatic potential (MESP) model was used to study specific molecular characteristics of organic dyes. Using their optimal configurations on the matching molecular surface, the electrostatic potential (ESP) maps of **F1-3** dyes are shown in Fig. 8. The ESP maps that are created here show the charge densities in the molecules in three dimensions. In terms of color, the areas of electrostatic potential usually rise in the correct sequence: blue > green > yellow > orange > red. However, regions of low potential (red color) and high potential (orange color) are distinguished by an excess of electrons and a shortage of electrons, respectively [45]. As can be seen in Fig. 8, F1 has a lower potential than the other dyes, suggesting the availability of electrons in the red portion of the structure.

3.4 Photovoltaic performance

Photovoltaic characterizations of co-sensitized devices were performed to establish the structure–property relationship and determine the best electron donating and anchoring groups for bichalcophene co-sensitizers system**s** on co-adsorption properties and establish a link between the co-adsorber structure and its corresponding solar performance. Photocurrent action spectra for bichalcophene co-sensitizers are depicted in Fig. 9. Impressively, as described in Table 3, the photovoltaic performance of the fabricated devices with 2-bichalcophene co-sensitizers **F1-3** was as follows: a photocurrent (J_{sc}) of 23.28, 19.96 and 21.31 (mA/cm^2); photovoltage (V_{oc}) of 0.733, 0.609 and 0.637 V; a fill factor (FF) of 58.40, 57.70 and 58.10%; and a PCE (η) of 9.97, 6.95 and 7.88%, respectively. The DSSC with **N-719** showed a *Jsc* of 20.71 mA. cm^{-2}, a V_{oc} of 0.586 eV, *FF* of 57.40%, and a PCE of 7.03%. (*I–V*) characteristics of the cell based on bichalcophene co-sensitizers F1-3 with N-719 are displayed in Fig. 9. Over co-sensitization, all the values of V_{oc} were improved, which suggests that the charge recombination caused by **N-719** aggregation is reduced by bichalcophene co-sensitizers **F1-3**, resulting in better performance of solar devices co-sensitized with **F1-3**. Besides the enhancement of the values of V_{OC}, the values of (FF) were also enhanced, which indicates that the smaller size of the bichalcophene co-sensitizers **F1-3** provides more sufficient covering of the TiO_2 surface [46, 47]. The efficiency of the **N-719** sensitized solar cell was lower than the co-sensitizers **F1-3** that indicates a sharper charge recombination produced from the closer π–π stacking or the dye aggregation [48]. The electron injection efficiency of the main complex dye **N-719** was reduced as a result of this aggregate. Following the addition of co-sensitizers to **N-719**, the efficiency was

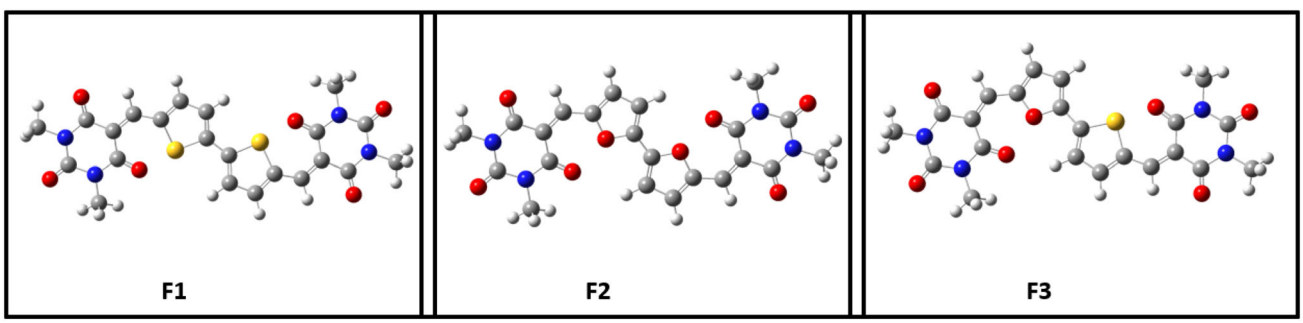

Fig. 6 Optimized structures for bichalcophene derivatives **F1-3**

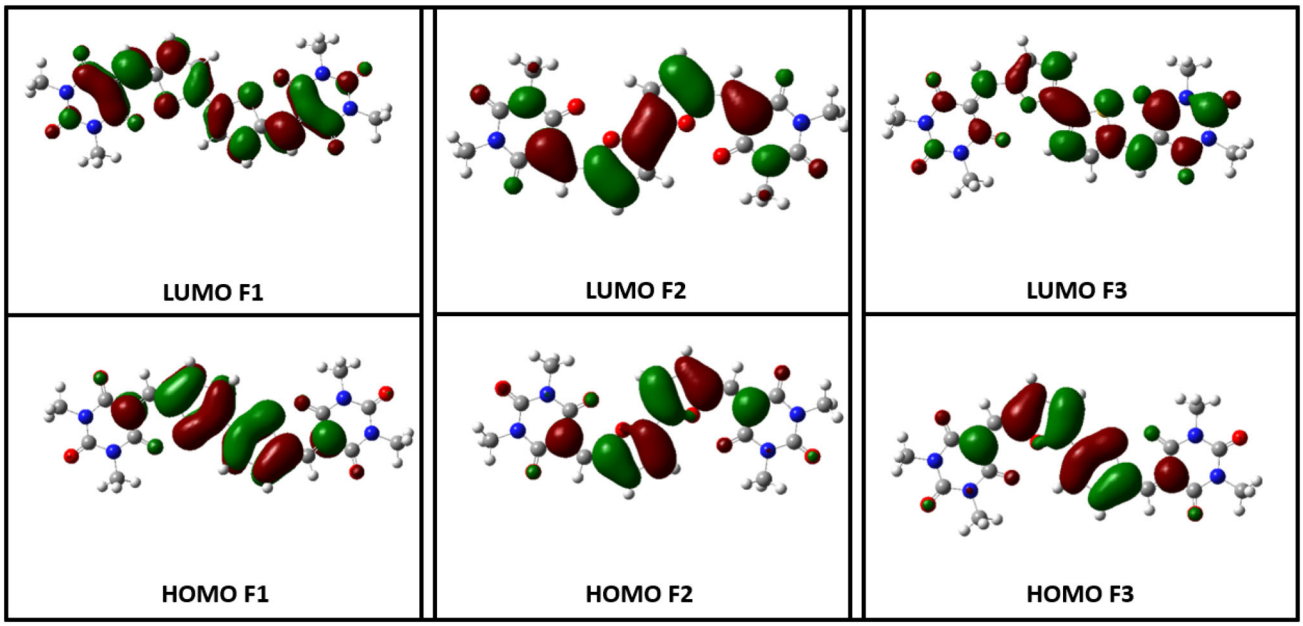

Fig. 7 Electron distribution on molecular orbital for bichalcophene derivatives **F1-3**

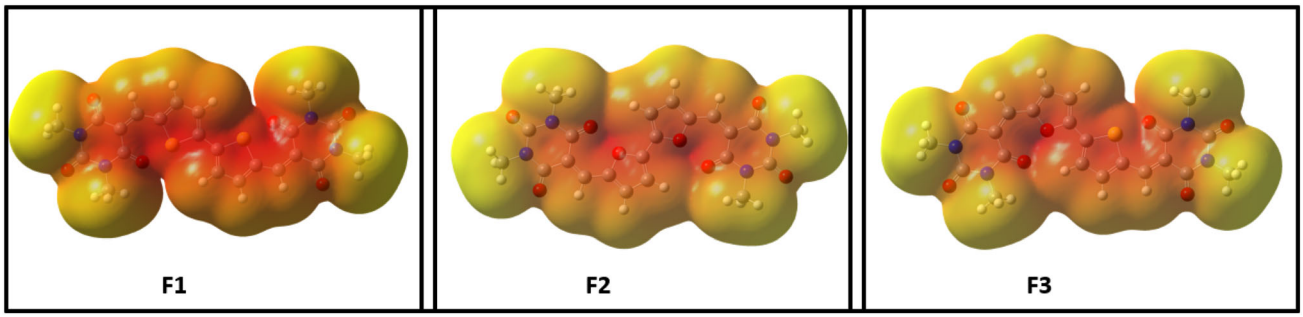

Fig. 8 MESP maps of bichalcophene structures **F1-3**

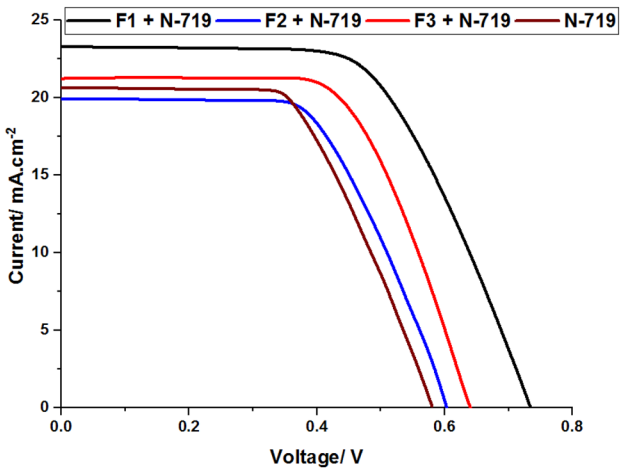

Fig. 9 *I–V* characteristics of solar devices based on bichalcophenes **F1-3 and N-719**

Table 3 Photovoltaic parameters of bichalcophene derivatives **F1-3**

Cell device	J_{SC} (mA cm^{-2})	V_{OC} (V)	FF (%)	η (%)
F1 + N-719	23.28	0.733	58.4	9.97
F2 + N-719	19.96	0.609	57.7	6.95
F3 + N-719	21.31	0.637	58.1	7.88
N-719	20.71	0.586	57.4	7.03
F1	10.66	0.654	64.3	4.41
F2	6.30	0.501	61.5	1.98
F3	6.99	0.557	62.4	2.43

improved. Thus, co-sensitizers are characterized by their small sizes, enabling for good, decreasing π–π stacking due to the presence thiophene/furan moiety. As a result, charge recombination is inhibited,

and device overall performance was improved [49]. In other circumstances, co-sensitizers should provide two roles: they should inhibit organic compounds from forming π–π stacking and they should also have a light harvesting ability. The PCE of the DSSCs fabricated with the bichalcophene co-sensitizers **F1-3** gradually increased in the following order: **N-719/F2** (6.95%) < **N-719/F3** (7.88%) < **N-719/F1** (9.97%). The highest efficiency was achieved with co-sensitizer **F1**, which is mainly related to the chemical structure of the bithiophene donor moiety/π-spacer**,** which will improve the solubility of the co-sensitizer suppressing the dark current. As a result, the highest value of V_{oc} of **F1** reflected a decreased electron recombination with a triiodide redox pair**.** On other hand, F1 showed the highest value of J_{SC} and showed the highest harvesting ability due to the highest molar extinction co-efficient and the most bathochromic shift in the absorption spectrum toward longer wavelengths.

For further confirmation of the abovementioned results, **F1-3** were fabricated, and their photovoltaic performances were measured individually without the standard dye **N-719**. Table 3 lists the photovoltaic characteristics associated with the *I–V* characteristic curves of **F1-3** seen in Fig. 10.

The fabricated devices **F1-3** displayed a maximum PCE (η) value for sensitizer **F1** of 4.41% (J_{SC} = 10.66 mA/cm^2, V_{OC} = 0.65 V, and FF = 64.30%) when compared to devices with **F2** (J_{SC} = 6.30 mA/cm^2, V_{OC} = 0.50 V, and FF = 61.5%), and **F3** (J_{SC} = 6.99 mA/cm^2, V_{OC} = 0.55 V and FF = 62.4%). The highest PCE value for **F1** as a sensitizer due to the highest values of V_{OC} and J_{SC}, which may be attributed to its effective anchoring property of 1,3-dimethyl barbituric acid and electron injection onto the TiO_2 surface. Poor performances of other dyes like **F2-3** can occur because of the lower molar extinction co-efficient of **F2-3** than **F1**, which had resulted in poor electron injection to the TiO_2 surface, further leading to lower J_{SC} values.

Furthermore, our results show that the photovoltaic performance of bichalcophene dyes **F1-3** follows the same patterns when co-sensitized with **N-719**. As a result, better sensitizers transferred to better co-sensitizers, confirming the higher performance.

(EIS) Electrochemical impedance spectroscopy is considered a helpful tool for analyzing the electron charge transfer and chemical capacitance at the TiO_2/dye/electrolyte and Pt/electrolyte interfaces in

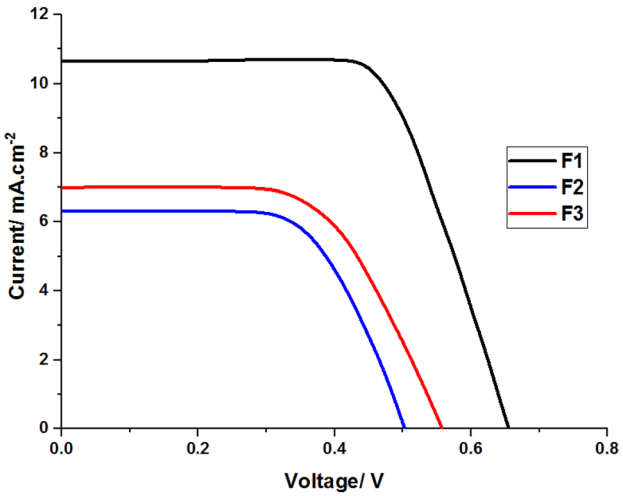

Fig. 10 *I–V* characteristics of solar devices based on bichalcophenes **F1-3**

DSSCs fabricated with sensitizers [50, 51]. Nyquist plots for co-sensitized cells based on bichalcophene co-sensitizers **F1-3** with the main dye **N-719** are displayed in Fig. 11. It had two distinct semicircles. The small semicircle at lower frequency represents the cathode charge transfer resistance, which is directly related to FF, and the large semicircle at middle frequency represents the charge recombination resistance (R_{ct}) from TiO_2 to the electrolyte, which is directly related to V_{oc}. In Nyquist plots, the radius of the large semicircle of the cells co-sensitized by **F1-3** was all larger than that sensitized by metal complex **N-719** only, **F1 + N-719 > F3 + N-719 > F2 + N-719 > N-719**. This clearly shows that the co-sensitization by bichalcophene co-sensitizers is beneficial in reducing dark current. As a result, Nyquist plots show that co-sensitization helps to suppress charge recombination at the TiO_2/dye/electrolyte interface. Co-sensitizers **F1-3** displayed larger R_{ct} in relation to **N-719** upon co-sensitization devices, due to the small structure of bichalcophene co-sensitizers characterized by various acceptors and anchoring moieties represented in (1,3-dimethylbarbituric acid) that are favorable for depressing undesired charge recombination, which is related to the ability of bichalcophene co-sensitizers to fill the dip from the main dye **N-719** and is clearly beneficial in reducing electron recombination and beneficial in reducing the dark current. The foregoing corresponds to the *V*oc values in Table 3. As a result, Nyquist plots show that co-sensitization helps to suppress charge recombination at the TiO_2/dye/electrolyte interface.

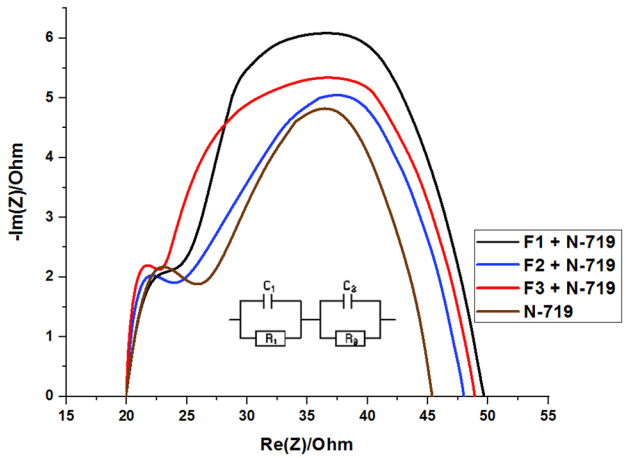

Fig. 11 Nyquist plots of bichalcophene derivatives **F1-3** and **N-719** based devices

4 Conclusion

Three organic dyes, denoted by the letters **F1**, **F2**, and **F3**, were created as sensitizers and co-sensitizers for dye-sensitized solar cells. These bichalcophene compounds were described and evaluated, and their optical and electrochemical parameters were examined. Furthermore, theoretical studies based on the DFT approach were used to investigate their photovoltaic properties. With a PCE of 4.41%, the bithiophene derivative **F1** had the highest DSSC efficiency in the photovoltaic characterization when sensitized as a single device. Furthermore, **F1, F2**, and **F3** were co-sensitized with a conventional Ru (II) dye, **N-719**, to promote light-harvesting across a wider spectral area and therefore enhance efficiency. The photovoltaic cell co-sensitized with **F1** surpassed the device using **N-719** alone, with an enhanced efficiency of 9.97%, a J_{SC} of 23.28 mA cm^{-2}, V_{OC} of 0.733 V, and a FF of 58.4% (an efficiency of 7.03% for **N-719**) owing to the maximum molar extinction coefficient complementing the light-harvest ability of **N719** dye. Further, the devices were subjected to electrochemical impedance spectroscopy to gain an insight into the interfacial charge transfer and recombination processes while in use. Finally, density functional theory (DFT) has been studied for bichalcophene dyes **F1-3** using Guassian09 software and the outcomes comfortably agree with experimental results.

Author contributions

FHA: synthesis, methodology, and graphical plots. MAI and EA-L: supervision, initial corrections, and comments. AAA: optical proprieties measurements, data analysis and revision. MRE: writing original draft, data analysis, editing, proofreading, and manuscript handling. All the authors read and approved the final manuscript.

Funding

The authors received no funding for this research.

Data availability

The data that support the findings of this study are available on request from the corresponding author.

Declarations

Conflict of interest The authors declare that they have no conflict of interest.

Supplementary Information: The online version contains supplementary material available at https://doi.org/10.1007/s10854-022-08470-9.

References

1. B. Oregan, M. Gratzel, A low-cost high-efficiency solar cell based on dye sensitized colloidal TiO_2 films. Nature **353**, 737–740 (1991)
2. M. Gratzel, Solar energy conversion by dye-sensitized photovoltaic cells. Inorg. Chem. **44**, 6841–6851 (2005)
3. A. Hagfeldt, G. Boschloo, L. Sun, L. Kloo, H. Pettersson, Dye-sensitized solar cells. Chem. Rev. **110**, 6595–6663 (2010)
4. X. Meng, C. Yu, X. Zhang, L. Huang, M. Rager, J. Hong, J. Qiu, Z. Lin, Active site senriched carbon matrix enables efficient triiodide reduction in dye-sensitized solar cells: an understanding of the active centers. Nano Energy **54**, 138–147 (2018)
5. X. Meng, C. Yu, X. Song, J. Iocozzia, J. Hong, M. Rager, H. Jing, S. Wang, L. Huang, J. Qiu, Z. Lin, Scrutinizing defects and defect density of selenium-doped Graphene for high-

efficiency triiodide reduction in dye-sensitized solar cells. Angew. Chem. Int. Ed. **130**, 4772–4776 (2018)
6. M. Barrera, I. Crivelli, B. Loeb, On the performance of ruthenium dyes in dye sensitized solar cells: a free cluster approach based on theoretical indexes. J. Mol. Model. **22**, 118 (2016)
7. S. Aghazada, M.K. Nazeeruddin, Ruthenium complexes as sensitizers in dye sensitized solar cells. Inorganics **6**, 52 (2018)
8. C. Woodward, T. Rüther, C. Coghlan, T. Jones, Y. Hebting, R. Cordiner, R. Dawson, D. Robinson, C. Forsyth, G. Wilson, Preparation of tetracarboxylated bis-bipyridine Ruthenium dyes: synthesis, structural and electronic characterization. Chem. Plus Chem. **83**, 691–703 (2018)
9. A. Sen, A. Gro, β effect of electron withdrawing/donating groups on the sensitizing action of the novel organic dye "3-(5-(4-(Diphenylamino)Styryl)Thiophen-2-Yl)-2-Cyanoacrylic Acid" for N-Type dye sensitized solar cells: a theoretical study. J. Phys. Chem. C **124**(16), 8526–8540 (2020)
10. A. Mishra, M.K.R. Fischer, P. Büuerle, Metal-free organic dyes for dye-sensitized solar cells: from structure: property relationships to design rules. Angew. Chem. Int. Ed. **48**(14), 2474–2499 (2009)
11. S. Singh, M. Chandrasekharam, K. Gupta, A. Islam, L. Han, G. Sharma, Co-sensitization of amphiphilic ruthenium(II) sensitizer with a metal free organic dye: improved photovoltaic performance of dye sensitized solar cells. Org. Electron. **14**, 1237–1241 (2013)
12. J. Luo, Z. Wan, C. Jia, Y. Wang, X. Wu, A co-sensitized approach to efficiently fill the absorption valley, avoid dye aggregation and reduce the charge recombination. Electrochim. Acta **215**, 506–514 (2016)
13. Y.-J. Chen, Y.-C. Chang, L.-Y. Lin, W.-C. Chang, S.-M. Chang, Enhancing the spectral response of mesoporous ZnO films of dye–sensitized solar cells by incorporating metal-free organic sensitizer and N719 dye. Electrochim. Acta **178**, 414–419 (2015)
14. A. Mishra, M. Fischer, P. Bäuerle, Metal-free organic dyes for dye-sensitized solar cells: from structure: property relationships to design rules. Angew. Chem. Int. Ed. **48**, 2474–2499 (2009)
15. Z. Ning, Y. Fu, H. Tian, Improvement of dye-sensitized solar cells: what we know and what we need to know. Energy Environ. Sci. **3**, 1170–1181 (2010)
16. M. Al-Eid, S. Limb, K. Park, B. Fitzpatrick, C. Han, K. Kwak, J. Hong, G. Cooke, Facile synthesis of metal-free organic dyes featuring a thienylethynyl spacer for dye sensitized solar cells. Dyes Pigm. **104**, 197–203 (2014)
17. R.Y.-Y. Lin, F.-L. Wu, C.-H. Chang, H.-H. Chou, T.-M. Chuang, T.-C. Chu et al., Y-shaped metal-free D–π–$(A)_2$ sensitizers for high-performance dye-sensitized solar cells. J. Mater. Chem. A **2**, 3092–3101 (2014)
18. S. Fernandes, M. Castro, D. Ivanou, A. Mendes, M. Raposo, Push-pull heterocyclic dyes based on pyrrole and thiophene: synthesis and evaluation of their optical, redox photovoltaic properties. Coatings **12**(1), 34 (2022)
19. K. Kavya, P. Naik, A. Adhikari, Simple thiophene based organic dyes as active photosensitizers for DSSC application: from molecular design to structure property relationship. J. Nano-Electron. Phys. **12**, 02039 (2020)
20. S. Rouhani, M. Hosseinnezhad, N. Sohrab, K. Gharanjig, A. Salem, Z. Ranjbar, Investigation of the effect of rGO/TiO_2 on photovoltaic performance of DSSCs devices. Prog. Color. Color. Coat **15**, 123–131 (2022)
21. L. Zhang, J. Cole, Anchoring groups for dye-sensitized solar cells. ACS Appl. Mater. Interfaces **7**, 3427–3455 (2015)
22. F. Ambrosio, N. Martsinovich, A. Troisi, Effect of the anchoring group on electron injection: theoretical study of phosphonated dyes for dye-sensitized solar cells. J. Phys. Chem. C **116**, 2622–2629 (2012)
23. B. Hosseinzadeh, A.S. Beni, A.N. Chermahini, R. Ghahary, A. Teimouri, Novel organic dyes with anchoring group of barbituric/thiobarbituric acid and their application in dye-sensitized solar cells. Synth. Met **209**, 1–10 (2015)
24. S. Badawy, R. Su, A. Fadda, E. Abdel-Latif, A. El-Shafei, M. Elmorsy, Highly efficient (N-benzothiazolyl)-cyanoacetamide based co-sensitizers for high efficiency dye-sensitized solar cells. Optik **249**, 168274 (2022)
25. K. Harmanda, K. Tavera, M. Gezgin, M. Nebioğlu, İ Şişman, G. Jirón, D. Atilla, A. Gürek, A new sterically hindered asymmetric zinc phthalocyanine as an efficient sensitizer for dye-sensitized solar cells. New J. Chem. **46**, 714–725 (2022)
26. M. Elmorsy, E. Abdel-Latif, S. Badawy, A. Fadda, New cyanoacetanilides based dyes as effective co-sensitizers for DSSCs sensitized with ruthenium (II) complex (HD-2). J. Mater. Sci. Mater. Electron. **31**, 7981–7990 (2020)
27. L. da Silva, M. Sánchez, M. Rodriguez, H. Freeman, Isomeric tetrazole-based organic dyes for dye-sensitized solar cells: structure-property relationships. J. Mol. Struct. **1250**, 131749 (2022)
28. M. Eltoukhi, A. Fadda, E. Abdel-Latif, M. Elmorsy, Low cost carbazole-based organic dye bearing the acrylamides and 2-pyridone moieties for efficient dye-sensitized solar cells. J. Photochem. Photobiol. A **426**, 113760 (2022)
29. S. Fernandes, M. Castro, L. Mesquita, L. Andrade, A. Mendes, M. Raposo, Synthesis and characterization of novel thieno [3, 2-b] thiophene based metal-free organic dyes with different heteroaromatic donor moieties as sensitizers for dye-sensitized solar cells. Dyes Pigm. **136**, 46–53 (2017)

30. D. Babu, R. Su, A. El-Shafei, A. Adhikari, From molecular design to cosensitization; High performance indole based photosensitizers for dye-sensitized solar cells. Electrochim. Acta **198**, 10–21 (2016)
31. M. Nazeeruddin, M. Zakeeruddin, R. Humphry-Baker, M. Jirousek, P. Liska, N. Vlachopoulos, M. Grätzel, Acid−Base equilibria of (2, 2 '-Bipyridyl-4, 4 '-dicarboxylic acid) ruthenium (II) complexes and the effect of protonation on charge-transfer sensitization of nanocrystalline titania. Inorg. Chem. **38**, 6298–6305 (1999)
32. Y. Shu, A. Mikosch, K.N. Winzenberg, P. Kemppinen, C.D. Easton, A. Bilic, C.M. Forsyth, C.J. Dunn, T.B. Singha, G.E. Collis, N-Alkyl functionalized barbituric and thiobarbituric acid bithiophene derivatives for vacuum deposited n-channel OFETs. J. Mater. Chem. C **2**(20), 3895–3899 (2014)
33. M.A. Ismail, M.H. Abdel-Rhman, G.A. Abdelwahab, W.S. Hamama, H.M. El-Shafeai, W.M. El-Sayed, Synthesis of new thienylpicolinamidine derivatives and possible mechanisms of antiproliferative activity. RSC Adv. **10**, 41165–41176 (2020)
34. M.S. McClure, F. Roschangar et al., A practical one-pot synthesis of 5-aryl-2-furaldehydes. Synthesis **11**, 1681–1685 (2001)
35. M.A. Ismail, D.W. Boykin, C.E. Stephens, An efficient synthesis of 5,5'-diaryl-2,2'-bichalcophenes. Tetrahedron Lett. **47**, 795–797 (2006)
36. A. Mishra, C. Ma, P. Bäuerle, Functional oligothiophenes: molecular design for multidimensional nanoarchitectures and their applications. Chem. Rev. **109**, 1141–1276 (2009)
37. Z. Iqbal, W.-Q. Wu, D.-B. Kuang, L. Wang, H. Meier, D. Cao, Phenothiazine-based dyes with bilateral extension of π-conjugation for efficient dye-sensitized solar cells. Dyes Pigm. **96**, 722–731 (2013)
38. J. Yang, P. Ganesan, J. Teuscher, T. Moehl, Y. Kim, C. Yi, P. Comte, K. Pei, T. Holcombe, M. Nazeeruddin, J. Hua, S. Zakeeruddin, H. Tian, M. Grätzel, Influence of the donor size in D-π-A organic dyes for dye-sensitized solar cells. J. Am. Chem. Soc. **136**, 5722–5730 (2014)
39. J. Luo, Z. Wan, C. Jia, Y. Wang, X. Wu, X. Yao, Co-sensitization of dithiafulvenyl-phenothiazine based organic dyes with N719 for efficient dye-sensitized solar cells. Electrochim. Acta **211**, 364–374 (2016)
40. H. Tian, X. Yang, J. Cong, R. Chen, C. Teng, J. Liu, Y. Hao, L. Wang, L. Sun, Effect of different electron donating groups on the performance of dye-sensitized solar cells. Dyes Pigm. **84**, 62–68 (2010)
41. Z.-S. Huang, H.-L. Feng, X.-F. Zang, Z. Iqbal, H. Zeng, D.-B. Kuang, L. Wang, H. Meier, D. Cao, Dithienopyrrolobenzothiadiazole-based organic dyes for efficient dye-sensitized solar cells. J. Mater. Chem. A **2**, 15365–15376 (2014)
42. J. Zhao, X. Yang, M. Cheng, S. Li, L. Sun, Molecular design and performance of hydroxylpyridium sensitizers for dye-sensitized solar cells. ACS. Appl. Mater. Interfaces **5**, 5227–5231 (2013)
43. M. Frisch, G.W. Trucks, H. Schlegel, G. Scuseria, M. Robb, J. Cheeseman, G. Scalmani, V. Barone, B. Mennucci, G.A. Petersson, H. Nakatsuji, M. Caricato, X. Li, H. P. Hratchian, A. F. Izmaylov, J. Bloino, G. Zheng, J.L. Sonnenberg, M. Hada, M. Ehara, K. Toyota, R. Fukuda, J. Hasegawa, M. Ishida, T. Nakajima, Y. Honda, O. Kitao, H. Nakai, T. Vreven, J. A. Montgomery Jr., J.E. Peralta, F. Ogliaro, M. Bearpark, J.J. Heyd, E. Brothers, K.N. Kudin, V.N. Staroverov, R. Kobayashi, J. Normand, K. Raghavachari, A. Rendell, J. C. Burant, S.S. Iyengar, J. Tomasi, M. Cossi, N. Rega, J.M. Millam, M. Klene, J. E. Knox, J. B. Cross, V. Bakken, C. Adamo, J. Jaramillo, R. Gomperts, R. E. Stratmann, O. Yazyev, A. J. Austin, R. Cammi, Eur. J. Inorg. Chem. 3690–3697 (2017), www.eurjic.org 3697 © 2017 Wiley-VCH Verlag GmbH & Co. KGaA, W. C. Pomelli, J. W. Ochterski, R. L. Martin, K. Morokuma, V. G. Zakrzewski, G. A. Voth, P. Salvador, J. J. Dannenberg, S. Dapprich, A. D. Daniels, Ö. Farkas, J. B. Foresman, J. V. Ortiz, J. Cioslowski, D. J. Fox, Gaussian 09, Revision A.02, Gaussian, Inc., Wallingford CT, 2009.
44. J.N. Clifford, E. Martínez-Ferrero, A. Viterisi, E. Palomares, Sensitizer molecular structure-device efficiency relationship in dye sensitized solar cells. Chem. Soc. Rev. **40**, 1635–1646 (2011)
45. M. Rashid, D. Hayati, K. Kwak, J. Hong, Theoretical investigation of azobenzene-based photochromic dyes for dye-sensitized solar cells. Nanomaterials **10**, 914 (2020)
46. Y.-J. Chen, Y.-C. Chang, L.-Y. Lin, W.-C. Chang, S.-M. Chang, Enhancing the spectral response of mesoporous ZnO films of dye-sensitized solar cells by incorporating metal-free organic sensitizer and N719 dye. Electrochim. Acta **178**, 414–419 (2015)
47. N. Neale, N. Kopidakis, J. van de Lagemaat, M. Grätzel, A. Frank, Effect of a coadsorbent on the performance of dye-sensitized TiO_2 solar cells: shielding versus band-edge movement. J. Phys. Chem. B **109**, 23183–23189 (2005)
48. M.R. Elmorsy, L. Lyu, E. Abdel-Latif, S. Badawy, A.M. El-Shafei, A. Fadda, Co-sensitization of HD-2 complex with low-cost cyanoacetanilides for highly efficient DSSCs. Photochem. Photobiol. Sci. **19**, 281–288 (2020)
49. P. Naik, R. Su, M.R. Elmorsy, A. El-Shafei, A.V. Adhikari, Investigation of new carbazole based metal-free dyes as active photosensitizers/co-sensitizers for DSSCs. Dyes Pigm. **149**, 177–187 (2017)

50. G. Oskam, B.V. Bergeron, G.J. Meyer, P.C. Searson, pseudohalogens for dye-sensitized TiO_2 photoelectrochemical cells. J. Phys. Chem. B **105**, 6867–6873 (2001)
51. Y. Hua, B. Jin, H. Wang, X. Zhu, W. Wu, M.-S. Cheung, Z. Lin, W.-Y. Wong, W.-K. Wong, Bulky dendritic triarylamine-based organic dyes for efficient co-adsorbent-free dye-sensitized solar cells. J. Power Sources **237**, 195–203 (2013)